CHEMISTRY OF MATERIALS
Cite This: Chem. Mater. 2019, 31, 1084−1091
Article
pubs.acs.org/cm

# Indium−Organic Frameworks Based on Dual Secondary Building Units Featuring Halogen-Decorated Channels for Highly Effective $CO_2$ Fixation

Yang Yuan,[†] Jiantang Li,[†] Xiaodong Sun,[†] Guanghua Li,[†] Yunling Liu,*[,†] Gaurav Verma,[‡] and Shengqian Ma*[,‡]

[†]State Key Laboratory of Inorganic Synthesis and Preparative Chemistry, College of Chemistry, Jilin University, Changchun 130012, P. R. China

[‡]Department of Chemistry, University of South Florida, 4202 East Fowler Avenue, Tampa, Florida 33620, United States

Supporting Information

**ABSTRACT:** With the utilization of a "bifunctional ligand-directed strategy", three isostructural indium−organic frameworks based on dual secondary building units (SBUs) were successfully constructed with targeted structures. In their frameworks, two types of unsaturated monomeric indium SBUs—$[In(OOC\text{-})_2(\text{-N-})X(H_2O)]$ and $[In(OOC\text{-})_2(\text{-N-})X_2]^-$ (X = Cl, Br, and I)—assemble to form 1D tubular channels with both open metal sites and weak base polarizing substituents. The trimeric indium SBUs $[In_3O(OOC\text{-})_6(DMA)_3]^+$ serve as robust external linkers to extend into a 3D honeycomb double-walled framework with nanoscale channels. By changing the polarizing substituents in situ with different halogens ($Cl^-$, $Br^-$, and $I^-$), three obtained isostructural MOFs show different channel characteristics, such as alkalinity of the polarizing substituents, acidity of the polarized open indium sites, extended channel sizes, and increased pore volumes (from -I to -Cl). Subsequently, we took the three MOFs collectively as a platform to investigate the impact of the different coordinated halide ions on channel functions, especially on $CO_2$ adsorption and chemical conversion. Accordingly, the three nanochannel MOF catalysts exhibited highly effective performances in catalyzing cycloaddition of $CO_2$ with large-sized epoxides, particularly styrene oxide, into value-added products—styrene carbonates with yields of 91−93% and high selectivity of 95−98%—under mild conditions. We speculated that the superior catalytic efficiencies of the three MOF catalysts could be ascribed to the synergistic effect of open indium sites as Lewis acid with different halide ions as weak base sites, which might enhance the catalytic selectivity through polarizing and activating $CO_2$ molecules during the reaction process.

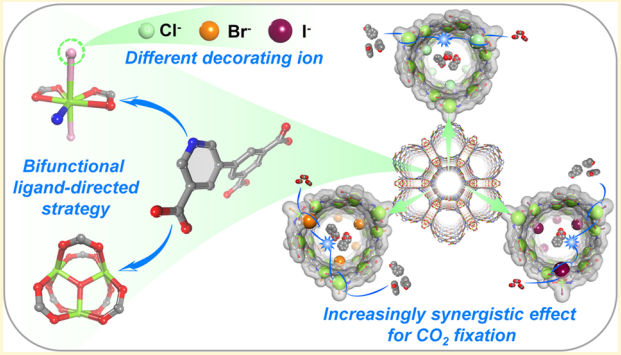


## INTRODUCTION

Metal−organic frameworks (MOFs), as structurally tunable porous materials, are built by integrating secondary building units (SBUs) and organic linkers. The variability of their two structural components endows MOFs a flexible design in both channel type and size, surface non-metallic active pendant groups, and open metal sites, which renders MOFs as outstanding functional porous materials ranging from $CO_2$ capture[1−3] to chemical fixation through heterogeneous catalysis.[4−24] To target a given application, classic design principles have been presented by synthetic MOF chemists[25−28] and diversely attractive SBUs have been constructed from various metal centers with different coordinated sites.[29]

Indium, as a high cycle p-block metal, has been attracting special interest for its unique electronic configuration, which endows it different binding affinities toward various coordinated atoms for "structure-directed synthesis".[30] Moreover, accessible high level p-orbitals enable it to easily receive electrons in various Lewis acidic reactions. Owing to these advantages, in the past decade, a large number of indium−organic frameworks (InOFs) have been synthesized with classic SBUs (such as tetrahedral $[In(OOC\text{-})_4]^-$ monomers displaying stable geometry and providing a local negative charge center,[31] $[In(OH)]$ chains,[32] and $[In_3O(OOC\text{-})_6]^+$ trimers,[33] which possess positive charge centers, a large number of In−O−In bonds and a corresponding high chemical stability) exhibiting interesting properties.[34−45] However, the single connected modes of indium SBUs have restrained the diversity of InOFs. InOFs with novel structures and fine-designed functionalization are still desirable in the rapidly evolving field of materials science. According to previous reports, designing MOFs by integrating multiple metal SBUs

Received: November 17, 2018
Revised: January 14, 2019
Published: January 15, 2019






DOI: 10.1021/acs.chemmater.8b04792
Chem. Mater. 2019, 31, 1084−1091

can not only greatly enrich the MOF structures but also display advantages of each kind of metal site.[30,36,46] However, the strategy of oriented integration of multiple metal SBUs into one framework has not yet been explored. On the other hand, although the "isoreticular synthesis" in situ could counter the post-synthesis damage to crystal frameworks, further design and tuning of pore functionalization in MOFs are largely limited by the organic synthesis techniques of similarly geometrical organic ligands as well as the disparities of coordination affinity of each ligands.[47,48] Alternative approaches for tuning pore functionalization are still highly desirable. Herein, we pay special attention to the nuance of coordination affinity between pyridyl nitrogen and carboxylate oxygen in directing the assembly of monomeric/trimeric indium SBUs. In particular, monomeric indium SBUs are likely to coordinate with carboxyl-O as well as pyridyl-N to maintain framework charge balance. On the contrary, in the trimeric indium SBUs, pyridyl-N could only serve as a terminal coordinate atom with larger steric hindrance than other terminal solvent atoms in addition to balancing the local charge.[49] Therefore, we speculate that pyridyl-N could be utilized to break the anionic carboxylate saturated monomeric indium configuration and construct novel SBUs with open metal sites. With the help of a "bifunctional ligand directed strategy" and by selecting 5-(3′,5′-dicarboxylphenyl)nicotinic acid ($H_3$DCPN) as a N,O-coordinated bifunctional ligand, we successfully integrated two types of unsaturated monomeric In SBUs and trimeric In cluster into one framework, which exhibited 3D honeycomb double-walled nanotubular channels. We further tuned the channels by shifting the surface terminal substituents with different halogens (-Cl, -Br, and -I). Consequently, three halogenated frameworks, denoted as InDCPN-X ( X = Cl, Br, and I), exhibited interesting structural characteristics, such as extended channel apertures and increased pore volume from -I to -Cl, different channel pendant polarizing groups (Cl, Br, and I), and the corresponding polarized open indium sites (Scheme 1).

**Scheme 1. Bifunctional Ligand, $H_3$DCPN, Directs Trimeric and Monomeric Indium SBUs To Form InDCPN-Cl, -Br, and -I with Different Polarizing Substituents Exposed in Their Channels. Color Code: In = Green, C = Gray, O = Red, N = Blue, Halogen = Pink, Cl = Cyan, Br = Orange, I = Purple, Indium Monomer = Blue Polyhedron, and Indium Trimer = Orange Polyhedron**

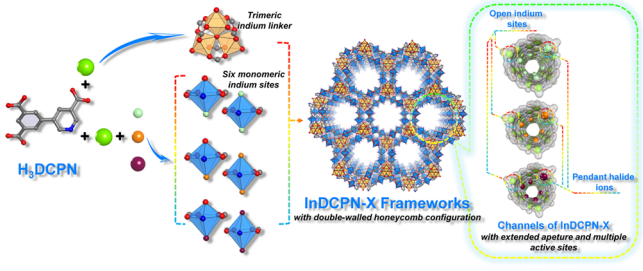


Subsequently, we took three different halogenated InDCPN-Xs collectively as a platform to evaluate the impact of their unique structural characteristics on channel functions especially in sequestering the rapidly increasing $CO_2$ emission by cycloaddition of $CO_2$ with epoxides into fine chemicals. Accordingly, these fine-designed structural characteristics, such as (1) the nanoscale columnar channels, (2) open monomeric In sites, (3) exposed polarizing substituents (Cl, Br, and I), and (4) robust trimeric indium linkers and double-walled honeycomb frameworks, rendered InDCPN-Xs as promising materials for catalyzing $CO_2$ fixation with high conversion and selectivity especially for large-sized substrates, outperforming some top-performing MOF catalysts.

## EXPERIMENTAL SECTION

**Materials and Methods.** PXRD data were collected using a Rigaku D/max-2550 diffractometer with Cu K$\alpha$ radiation ($\lambda$ = 1.5418 Å). Elemental analyses data (C, H, and N) were attained on a PerkinElmer 240 analyzer. FTIR data were obtained using a Nicolet Impact 410 FTIR spectrometer. XPS measurements were executed on an ESCALAB 250 X-ray photoelectron spectrometer, using Mg K$\alpha$ X-rays as the excitation source. ICP-OES analyses were performed on a PerkinElmer Optima 3300 DV spectrometer. TGA was carried out with a PerkinElmer TGA thermogravimetric analyzer under air flow in the range of 30−800 °C with a heating rate of 10 °C $min^{-1}$ for all the measurements. GC−MS analysis was carried out on Shimadzu GCMS-QP 2010 plus with a DB-5MS capillary column (30 m × 0.25 mm × 0.25 $\mu$m; J&W Scientific, Folsom, CA, USA). $^1$H NMR spectra were collected on a Varian 300 MHz NMR spectrometer. The $N_2$ adsorption measurements were carried out using Micromeritics ASAP 2420. $CO_2$, $CH_4$, $C_2H_6$, and $C_3H_8$ adsorption measurements were performed with a Micromeritics 3Flex instrument. Before carrying out the gas adsorption measurements, the samples were soaked in ethanol, and the ethanol was exchanged every 8 h for 5 days to completely remove the nonvolatile guest molecules. The samples were then subjected to dynamic vacuum at room temperature for 1 h and activated with the outgas function of the surface area analyzer for 10 h at 180 °C.

**Synthesis of InDCPN-Cl.** A mixture of $InCl_3{\cdot}4H_2O$ (60 mg, 0.2 mmol) and $H_3$DCPN (12 mg, 0.04 mmol) in DMA (1.5 mL) and $H_2O$ (0.6 mL) was sealed in a 20 mL capped vial, stirred for 1 h, and heated in an oven at 115 °C for 48 h. The solution was then cooled down to room temperature, and colorless rod-like single crystals were obtained. Yield: 66% (based on $H_3$DCPN). Elemental analysis (%) calc. for InDCPN-Cl: C, 38.36; H, 4.31; N, 6.52; found: C, 39.02; H, 4.87; N, 7.13.

**Synthesis of InDCPN-Br.** $In(OH)_3$ (30 mg, 0.18 mmol), concentrated hydrobromic acid (25 $\mu$L), and DMA (1 mL) were mixed in a 20 mL capped vial and stirred for 1 h resulting in a colorless solution to which $H_3$DCPN (9 mg, 0.03 mmol) was added. The mixture was sealed and heated in an oven at 120 °C for 48 h. It was then cooled down to room temperature to give colorless rod-like single crystals. Yield: 60% (based on $H_3$DCPN). Elemental analysis (%) calc. for InDCPN-Br: C, 35.89; H, 4.03; N, 6.10; found: C, 36.11; H, 4.17; N, 6.23.

**Synthesis of InDCPN-I.** A mixture of $InI_3$ (30 mg, 0.06 mmol) and $H_3$DCPN (3 mg, 0.01 mmol) in DMA (1 mL) was sealed in a 20 mL capped vial, stirred for 1 h, and then heated at 120 °C for 48 h. The solution was then cooled down to room temperature, and colorless rod-like single crystals were obtained. Yield: 62% (based on $H_3$DCPN). Elemental analysis (%) calc. for InDCPN-I: C, 34.63; H, 4.09; N, 6.21; found: C, 34.51; H, 3.98; N, 6.09.

The experimental PXRD patterns of the three products were in good agreement with the simulated patterns based on the single-crystal X-ray data, which indicated the bulk phase purity of the as-synthesized products (Figures S1−S3).

**X-ray Crystallography.** Crystallographic data for the three products were harvested using a Bruker Apex II CCD diffractometer equipped with graphite-monochromated Mo K$\alpha$ ($\lambda$ = 0.71073 Å) radiation at room temperature. All the structures were solved by the direct methods and refined by full-matrix least squares on $F^2$ using SHELXTL-NT version 5.1. All the metal atoms were first located. The carbon, oxygen, nitrogen, and halogen atoms of the compounds were subsequently found in difference Fourier maps. The hydrogen atoms of the ligand were placed geometrically. All non-hydrogen atoms were refined anisotropically. The final formulas of the three


DOI: 10.1021/acs.chemmater.8b04792
Chem. Mater. 2019, 31, 1084−1091

compounds were derived from the crystallographic data combined with the elemental and TGA data. The detailed crystallographic data and selected bond lengths and angles for InDCPN-Xs are listed in Tables S4–S6, respectively. Topology information for InDCPN-Xs was calculated using TOPOS 4.0.[50]

**Catalytic Performance Evaluation.** In a typical experiment, the catalytic reactions under 1 atm were performed in a 10 mL Schlenk tube charged with the epoxide (20 mmol), catalyst (0.01 mmol, 0.05 mol %), and tetra-*n*-butylammonium bromide (TBAB, 5 mol % for the optimized condition) as the co-catalyst. The catalytic reactions under high pressure (2 MPa) were performed in a 25 mL autoclave charged 5 times with epoxide and catalyst with/without TBAB as a co-catalyst. The mol % of the catalyst was based on the molecular weight of the activated compounds: $[In(DCPN)_{3/4}X_{7/6}]_6[In_3O(DCPN)_{3/2}]$ (according to the four coordinated sites of one DCPN, the ligand was viewed as four parts to coordinate with indium SBUs in the expression above). After sealing, the reactor was purged with $CO_2$. The reaction mixture was then stirred under mild conditions (25 °C for propylene oxide and 80 °C for the large-sized epoxides) for a given period of time. The catalysts were separated by centrifugation and activated again for reuse. The products were detected by $^1H$ NMR.

## RESULTS AND DISCUSSION

**Characterization of Crystal Structures.** The single-crystal XRD analysis revealed that the three InDCPN-Xs were isostructural with a difference in the channel-pendant ions ($Cl^-$, $Br^-$, and $I^-$). In their frameworks, carboxyl-O assembled trimeric In SBUs: $[In_3O(OOC\text{-})_6(DMA)_3]^+$, and two types of pyridyl-N directly assembled monomeric In SBUs: $[In(OOC\text{-})_2(\text{-N-})(H_2O)X]$ and $[In(OOC\text{-})_2(\text{-N-})X_2]^-$ are coexistent. A 1D nanotubular channel with an aperture of ~18 Å is constructed by the 3-connected indium monomer (simplified as triangle, Figure 1a), further connected with trimeric indium SBUs externally (Figure 1b). The 6-connected indium trimer (simplified as triangular prism) acts as a robust linker to connect three adjacent channels to form a 3D honeycomb dual-indium SBU based framework with double-walled nanoscale channels along the *c*-direction (Figure 1c). This configuration along *c* displays the stable geometry similar to the MCM-41 zeolite. Additionally, the $DCPN^{3-}$ ligand can be simplified as a 4-connected rectangle (Figure 1a). Therefore, from a topological point of view, the framework can be classified into a 3,4,6-connected new topology (Figure 1d). To the best of our knowledge, only two MOFs in the literature contain both monomeric and trimeric indium SBUs,[51,52] and their monomeric sites are saturated 8-coordinated carboxylate SBUs. InDCPN-Xs represent the first MOFs to integrate open monomeric indium sites with trimeric clusters into one framework. Moreover, the design process of employing bifunctional ligands to directly assemble unsaturated N/O-coordinated monomeric/trimeric hybrid InOFs may provide a fruitful route for achieving the desired novel functional porous materials.

The indium monomers in InDCPN-Xs exhibit two rare pyridyl-N participating 7-coordination configurations with different terminal substituents, denoted as neutral $[In(OOC\text{-})_2(\text{-N-})(H_2O)X]$ and anionic $[In(OOC\text{-})_2(\text{-N-})X_2]^-$. Each central indium ion of both types of SBUs is coordinated with two pairs of carboxylate oxygen, one pyridyl nitrogen in the channel wall plane, and additional two terminal atoms that are coordinated perpendicularly. The ones pointing toward the channel center are all halogens, while the opposite ones are either halogens or oxygen (from water). According to the crystallographic data, the two kinds of inside terminal atoms

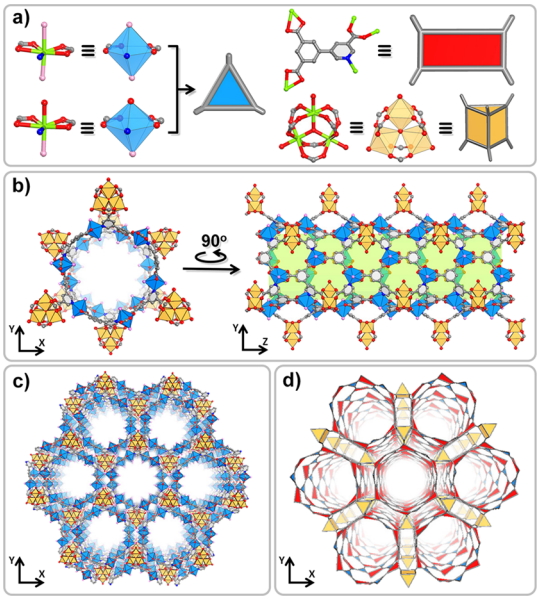


**Figure 1.** Crystal structure of InDCPN-Xs. (a) Integration of triangular monomeric indium SBUs $[In(OOC\text{-})_2(\text{-N-})(H_2O)X]^-$ and $[In(OOC\text{-})_2(\text{-N-})X_2]$ and trigonal-prismatic trimeric indium SBUs $[In_3O(OOC\text{-})_6(DMA)_3]^+$ and rectangular $DCPN^{3+}$ results in (b) the nanotubular channel with the external linkers; (c) the structure of InDCPN-Xs; (d) the structure displays a new 3,4,6-connected topology. Color code: In = green, C = gray, O = red, N = blue, halogen = pink, indium monomer = blue polyhedron, and indium trimer = orange polyhedron. All H atoms are omitted for clarity.

have occupancies of 5/6 and 1/6 to form $[In(OOC\text{-})_2(\text{-N-})(H_2O)X]$ and $[In(OOC\text{-})_2(\text{-N-})X_2]^-$, respectively (Figure 2).

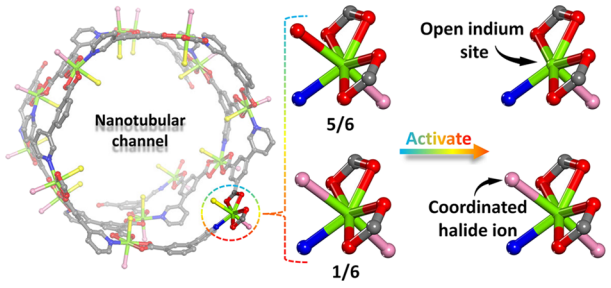


**Figure 2.** Two types of monomeric indium SBUs that constructed the 1D channel of InDCPN-X: $[In(OOC\text{-})_2(\text{-N-})(H_2O)X]^-$ with an occupancy of 5/6 and which has exposed open metal sites as Lewis acid sites through the activation process and $[In(OOC\text{-})_2(\text{-N-})X_2]$ with an occupancy of 1/6 and which carried different halide ions as weak Lewis basic sites. Color code: In = green, C = gray, O = red, N = blue, halogen = pink, inside terminal coordinated molecule (water or halogen) = yellow. All H atoms are omitted for clarity.

The aqua ligand of $[In(OOC\text{-})_2(\text{-N-})(H_2O)X]$ can be thermally liberated (180 °C, vacuum, degassed for 10 h) to expose the active open indium sites, as supported by the TGA analyses of the activated InDCPN-X samples (Figures S4–S6). Meanwhile, the halogen ligands remain on the SBUs (supported by the XPS analyses in Figure S7) to maintain a localized negatively charged center beneficial for polarizing $CO_2$.[51,53] The three MOFs have solvent accessible volumes of 62.8, 61.7, and 58.4% for InDCPN-Cl, -Br, and −I, respectively, and possess high densities of two types of active


DOI: 10.1021/acs.chemmater.8b04792
*Chem. Mater.* 2019, 31, 1084–1091

sites, which are 10 open monomeric indium sites and 2 polarizing halide ions per unit cell. As shown in Scheme 1, the two monomeric SBUs are divided into six active binding sites based on the different coordinated halide ions: the neutral $[In(OOC\text{-})_2(\text{-N-})(H_2O)Cl]$, $[In(OOC\text{-})_2(\text{-N-})(H_2O)Br]$, and $[In(OOC\text{-})_2(\text{-N-})(H_2O)I]$ with different polarized open indium sites as Lewis acidic sites; and the anionic $[In(OOC\text{-})_2(\text{-N-})Cl_2]^-$, $[In(OOC\text{-})_2(\text{-N-})Br_2]^-$, and $[In(OOC\text{-})_2(\text{-N-})I_2]^-$ carrying different halide ions as weak Lewis bases with different alkalinity. Additionally, the In−X bond lengths in $[In(OOC\text{-})_2(\text{-N-})X_2]^-$ were measured to be 2.57, 2.82, and 3.00 Å for InDCPN-Cl, InDCPN-Br, and InDCPN-I, respectively. Accordingly, a shrinkage of their channel apertures from 12.93 to 11.59 Å was observed. Notably, this approach of tuning channel properties by employing halide ions with similar coordination affinities may also represent a convenient and easy route for the pore functionalization of porous materials.

**Gas Adsorption and Separation Behavior.** The permanent porosity of activated InDCPN-Cl, -Br, and -I was proven by $N_2$ adsorption isotherms at 77 K (Figure 3a). All of

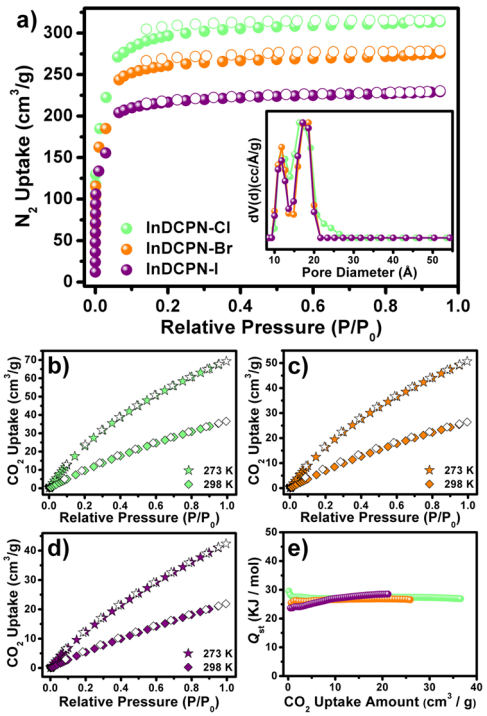


**Figure 3.** (a) $N_2$ adsorption isotherms at 77 K and pore size distribution calculated by the NLDFT method, in which the peaks are matched with the channel apertures of 11.5−13.0 and 17.6−18.1 Å (inset). The $CO_2$ adsorption isotherms of the activated (b) InDCPN-Cl, (c) -Br, and (d) -I at 273 and 298 K. (e) The corresponding $Q_{st}$ plots.

them revealed a steep $N_2$ uptake in the low-pressure region ($P/P_0 < 0.06$), with the resulting profiles of fully reversible type-I isotherms characteristic of microporous materials. The BET surface areas of InDCPN-Cl, -Br, and -I were estimated to be 997, 875, and 726 $m^2\ g^{-1}$ (Langmuir surface areas of 1351, 1174, and 972 $m^2\ g^{-1}$), respectively, and compared with their space volumes and main channel diameters according to the structural characteristics. The pore size distribution of the InDCPN-X series was examined by fitting the NLDFT models to their 77 K $N_2$ adsorption isotherms (Figure 3a, inset). The calculated apertures were in good agreement with the two types of channel sizes observed from their single-crystal structures—the channel diameter without terminal molecules (17.6−18.1 Å) and decorated with halogens (11.5−13.0 Å).

After proving their permanent porosity, adsorption of various gases such as $CO_2$ and some light alkanes was performed to evaluate the difference in their channel properties resulting from different decorated halogens (from $[In(OOC\text{-})_2(\text{-N-})X_2]^-$) and the corresponding halogenated open indium centers (from the activated monomeric indium SBU $[In(OOC\text{-})_2(\text{-N-})X]$). The MOFs exhibited regular changes in adsorption performances of various gases (Figures S9−S20 and Tables S3 and S4). We took special interest in their $CO_2$ adsorption behaviors because of the possible interactions of $CO_2$ with the open indium sites and weak basic polarizing centers (coordinated halide ions) modified on the channel surface. Accordingly, the $CO_2$ sorption isotherms of the InDCPN-X series at 273 and 298 K were measured (Figure 3b). The saturated adsorption amounts of InDCPN-Cl, -Br, and -I were 69, 50, and 42 $cm^3\ g^{-1}$ at 273 K (35, 26, and 21 $cm^3\ g^{-1}$ at 298 K), respectively. The corresponding isosteric heats of $CO_2$ adsorption ($Q_{st}$) at zero coverage were calculated to be 30, 26, and 24 kJ $mol^{-1}$, respectively, by fitting the $CO_2$ isotherms at 273 and 298 K with the virial method. The difference in $CO_2$ adsorption amount can be attributed to the synergy of their different surface areas and $CO_2$ affinities as shown by the different zero coverage $Q_{st}$ values.

The higher $Q_{st}$ of InDCPN-Cl than the other two may result from the relatively strong alkalinity of chloride ions among the three halogens. The order of the $CO_2$ adsorption of the InDCPN-X series led us to carry out the subsequent studies for their catalytic behavior toward $CO_2$ chemical conversion.

**Catalytic Cycloaddition of $CO_2$ with Epoxides.** Cycloaddition of $CO_2$ with epoxides to targeted value-added chemicals has become a highlighted reaction for sequestering the sharp increase in $CO_2$ emissions. The reaction process can be effectively facilitated by weak Lewis acidic and basic sites. In particular, the weak Lewis sites can activate the substrates not only by polarizing the epoxides and the $CO_2$ molecules but also through easier release of the activated substrates compared to the stronger Lewis sites.[54] By virtue of the diffusion-facilitated nanotubular channels, accessible monomeric open indium sites, and weak basic halide ions of InDCPN-Xs, we thus took the three MOFs collectively to evaluate their catalytic performances in the cycloaddition reaction as well as study the effect of their different pendant halide ions. First, we selected transforming styrene oxide with $CO_2$ into styrene carbonate as a model reaction in consideration of the substrate-matched compound channels and the possible facilitations of the weak basic sites to the reported insufficient catalytic selectivity of the substrate.[24] Accordingly, under relatively mild conditions (1 atm and 80 °C) and over a period of 24 h, the three MOF catalysts exhibited highly effective catalytic efficiencies with yields of 91−93% and selectivities of 95−98% (Table 1, entries 2, 5, and 6). These values are much higher than the traditional acid/base-based MOF materials as well as some of the other heterogeneous/homogeneous catalysts as shown in Table S8. Moreover, these yields are comparable to some of the recently reported top-performing MOF catalysts (as shown in Table S9), such as Hf-NU-1000 (100%),[12] Cu-TPTC-$NH_2$ (89%),[21] PCN-700-o (83%),[14] and MOF-892 (82%)[24] under similar conditions. In view of the


DOI: 10.1021/acs.chemmater.8b04792
Chem. Mater. 2019, 31, 1084−1091

**Table 1. Optimum Conditions for Cycloaddition of Carbon Dioxide with Styrene Epoxide Catalyzed by InDCPN-X Series[a]**

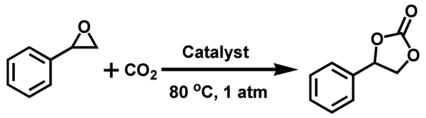


| entry | catalyst | T, h | con., %[b] | sel., %[b] | yield, %[b] |
|---|---|---|---|---|---|
| 1 | InDCPN-Cl | 12 | 72 | 98 | 71 |
| 2 | InDCPN-Cl | 24 | 95 | 98 | 93 |
| 3 | InDCPN-Cl[c] | 24 | 94 | 94 | 88 |
| 4 | InDCPN-Cl[d] | 24 | 86 | 97 | 84 |
| 5 | InDCPN-Br | 24 | 95 | 97 | 92 |
| 6 | InDCPN-I | 24 | 96 | 95 | 91 |
| 7 | InDCPN-Cl[e] | 4 | 95 | >99 | 95 |
| 8 | InDCPN-Cl[f] | 4 | <10 | | |
| 9 | none | 24 | 33 | 84 | 28 |

[a]Reaction conditions: 20 mmol styrene oxide (100 mmol in high-pressure reactions), 0.05 mol % InDCPN-X, and 5 mol % TBAB ($nBu_4NBr$) under 1 atm $CO_2$ at 80 °C. [b]Conversion (con.), selectivity (sel.), and percent yield were determined by $^1H$ NMR and GC−MS. [c]InDCPN-Cl (0.025 mol %). [d]TBAB (1 mol %). [e]2 MPa, 4 h. [f]2 MPa, 4 h without co-catalyst.

crystal structures, we ascribed this superior performance partially to the high density of easily accessible monomeric open indium sites and halide ions (10 and 2 per unit cell) hanging on the channel surface. Compared with MOF-892, the specialized catalyst for styrene oxide, the catalytic sites in one unit cell are 4 exposed Zr sites and 2 −OH groups within the conglomerate $[Zr_6O_4(OH)_4(CH_3CO_2)_6(\text{-}CO_2)_6]$ cluster.

To study the particular effect of the catalysts during the reaction process, control experiments with different parameters were carried out using InDCPN-Cl. Under the same conditions except a less amount of catalyst (0.025 mol %), the catalytic conversion showed no significant variation, while the selectivity decreased to 94% (Table 1, entry 3). On the other hand, using a smaller amount of the co-catalyst (1 mol %), the conversion decreased to 86%, while the selectivity was maintained (Table 1, entry 4). These two control batches revealed the effective promotion of our catalyst for catalytic selectivity, which can be attributed to the possible activation of the weak basic coordinated chloridion to easily polarize and release the epoxide ring and $CO_2$ during the catalytic process. In the batch without InDCPN-Cl, the conversion and selectivity were only 33 and 84%, respectively (Table 1, entry 9), which demonstrated the significant importance of InDCPN-Cl during the catalytic process. Under high pressure conditions (2 MPa, 80 °C, and 4 h), 0.05 mol % InDCPN-Cl with TBAB promoted the reaction to a yield of 95% and selectivity up to 99% (Table 1, entry 7), which was better than some reported efficient MOF catalysts such as gea-MOF-1 (85% yield, 2 MPa, 120 °C, 6 h)[9] under similar conditions. However, according to the batch without the co-catalyst, a less than 10% yield was observed (Table 1, entry 8), which suggested that the coordinated chloridion was bound and of less nucleophilicity and a nucleophilic co-catalyst was needed in the catalytic process. Moreover, the impact of different coordinated halide ions on the catalytic activity was found to be in an increasing order from InDCPN-I to -Cl. We speculated that it could possibly be ascribed to the increasing affinities of the coordinated $I^-$, $Br^-$, and $Cl^-$ with $CO_2$ molecules, which has been revealed by the $Q_{st}$ values of the three MOFs for $CO_2$. Additionally, the disagreement against the reported active rule of co-catalytic basic ions ($Br^- > I^- > Cl^-$)[55] suggests that, instead of acting like nucleophiles to attack the $\beta$-C of the epoxide ring, the coordinated halide ions are more likely to activate $CO_2$ molecules as weak Lewis basic sites in the polarizing and releasing process.

The regeneration ability is essential for a catalyst to reduce the cost of the process for industrial application. As shown in Figure S30, after five cycles of repeated catalytic measurements, InDCPN-Xs can still maintain their catalytic yields without a significant decrease. Meanwhile, the PXRD patterns of the 5 times recycled catalysts (Figures S27−29) and the ICP-OES analysis of the fifth product filtrate catalyzed by three InDCPN-X catalysts (Table S7), which indicated the $In^{3+}$ concentration is less than 0.1 ppm, also confirm that InDCPN-Xs are a series of robust and reusable heterogeneous MOF catalysts.

Subsequently, the catalytic performances for various epoxides were evaluated under similar optimized conditions with InDCPN-Cl, the most efficient catalyst in the series. Owing to its nanoscale channels, InDCPN-Cl also exhibited very high activities for the substrates of different sizes (Table 2), ranging from the smallest one, propylene oxide (4.2 × 2.6 Å, 89% yield), to the large substrates, cyclohexene oxide (5.1 × 3.9 Å, 90% yield) and benzyl phenylglycidyl ether (9.4 × 4.3 Å, 88% yield).

**Table 2. Catalytic Performance of InDCPN-Cl[a] for Cycloaddition of Carbon Dioxide with Various Epoxides**

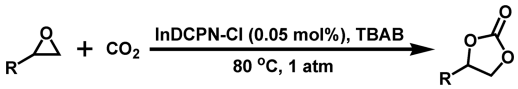


| Entry | Epoxide | Product | Yield /%[b] |
|---|---|---|---|
| 1 |  |  | 89 |
| 2 |  | 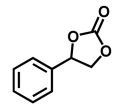 | 93 |
| 3 | 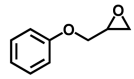 | 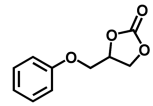 | 88 |
| 4 |  | 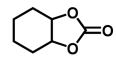 | 90 |

[a]Reaction conditions: epoxide (20 mmol), InDCPN-Cl (0.05 mol %), and TBAB (5 mol %) under 1 atm $CO_2$, 80 °C (25 °C for propylene oxide), and 24 h. [b]The percent yields were determined by $^1H$ NMR and GC−MS.

Based on the previously reported literature[54,55] and the crystal structures of InDCPN-Xs, an assumptive mechanism for the catalytic process was proposed (Figure 4). First, the open indium sites of InDCPN-Xs are involved in attracting and coordinating with the oxygen atom of the epoxide, further polarizing the epoxide ring. Then, the polarized ring receives a nucleophilic attack by the $Br^-$ of TBAB to form an open ring with an intermediate oxygen anion. The oxygen anion rapidly attacks the adjacent $CO_2$ molecule, which has been attracted and polarized by the weak Lewis basic site on the channel


DOI: 10.1021/acs.chemmater.8b04792
Chem. Mater. 2019, 31, 1084−1091

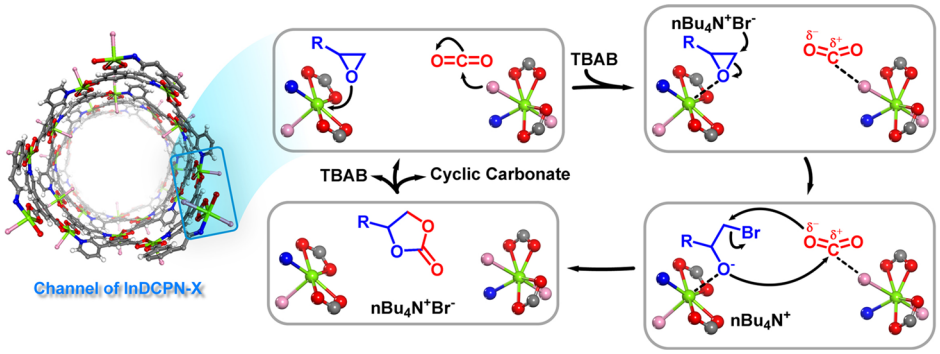


**Figure 4.** Tentatively proposed catalytic mechanism for the cycloaddition of epoxides and $CO_2$ into cyclic carbonates catalyzed by InDCPN-Xs. Color code: In = green, C = gray, O = red, N = blue, halogen = pink, and H = white.

surface of the MOF. Simultaneously, the oxygen from the polarized $CO_2$ attacks the epoxide carbon atom coordinated to $Br^-$, to finish the cyclization. Accordingly, it can be inferred that the overall cycloaddition process can be promoted synergistically by the weak Lewis acidic and basic sites incorporated within one framework.[8,16]

## CONCLUSIONS

In summary, we demonstrated a bifunctional ligand directed strategy to integrate two indium SBUs into one framework and form three isostructural MOFs with the desired structures. The new MOFs combine the advantages of the two metal SBUs—modifiable terminal coordinated ions as well as open metal sites of the monomeric indium SBUs and robust stability of the trimeric indium SBUs as linkers. By further modification with Cl, Br, and I anions, the target-designed InDCPN-X series exhibits enhanced channel properties especially for efficient $CO_2$ fixation with large-sized epoxides under relatively mild conditions. The influence of decorated halogens and their synergistic effect with open metal sites were proposed and studied, which showed some new avenues for designing of Lewis acids/bases incorporating MOFs for $CO_2$ fixation. The two design steps also present a fresh view in constructing MOFs incorporating multiple SBUs with "hybrid vigor" and exhibiting different pore characteristics to systematically explore the effect of some specific active centers.

## ASSOCIATED CONTENT

### Supporting Information

The Supporting Information is available free of charge on the ACS Publications website at DOI: 10.1021/acs.chemmater.8b04792.

Synthesis and characterization details, crystal structure and data, PXRD, TGA, gas sorption isotherms, FTIR spectra, 1H NMR, and catalytic reaction details (PDF)

Crystallographic data for InDCPN-Cl CCDC 1849249 (CIF)

Crystallographic data for InDCPN-Br CCDC 1849250 (CIF)

Crystallographic data for InDCPN-I CCDC 1849248 (CIF)

## AUTHOR INFORMATION

### Corresponding Authors

*E-mail: yunling@jlu.edu.cn (Y.L.).
*E-mail: sqma@usf.edu (S.M.).

### ORCID

Jiantang Li: 0000-0002-8963-5402
Guanghua Li: 0000-0003-3029-8920
Yunling Liu: 0000-0001-5040-6816
Shengqian Ma: 0000-0002-1897-7069

### Author Contributions

The manuscript was written through contributions of Y.Y., Y.L., and S.M. All authors have given approval to the final version of the manuscript.

### Notes

The authors declare no competing financial interest.

## ACKNOWLEDGMENTS

The authors gratefully acknowledge the financial support provided by the National Natural Science Foundation of China (No. 21771078, 21671074, and 21621001), the 111 Project (B17020), and the National Key Research and Development Program of China (2016YFB0701100).

## REFERENCES

(1) Yu, J.; Xie, L.-H.; Li, J.-R.; Ma, Y.; Seminario, J. M.; Balbuena, P. B. $CO_2$ Capture and Separations Using MOFs: Computational and Experimental Studies. *Chem. Rev.* **2017**, *117*, 9674−9754.

(2) Sumida, K.; Rogow, D. L.; Mason, J. A.; McDonald, T. M.; Bloch, E. D.; Herm, Z. R.; Bae, T.-H.; Long, J. R. Carbon Dioxide Capture in Metal−Organic Frameworks. *Chem. Rev.* **2012**, *112*, 724−781.

(3) Trickett, C. A.; Helal, A.; Al-Maythalony, B. A.; Yamani, Z. H.; Cordova, K. E.; Yaghi, O. M. The Chemistry of Metal−Organic Frameworks for $CO_2$ Capture, Regeneration and Conversion. *Nat. Rev. Mater.* **2017**, *2*, 17045.

(4) Li, B.; Chrzanowski, M.; Zhang, Y.; Ma, S. Applications of Metal-Organic Frameworks Featuring Multi-Functional Sites. *Coord. Chem. Rev.* **2016**, *307*, 106−129.

(5) Niu, Z.; Gunatilleke, W. D. C. B.; Sun, Q.; Lan, P. C.; Perman, J.; Ma, J.-G.; Cheng, Y.; Aguila, B.; Ma, S. Metal-Organic Framework Anchored with a Lewis Pair as a New Paradigm for Catalysis. *Chem* **2018**, *4*, 2587−2599.

(6) He, H.; Perman, J. A.; Zhu, G.; Ma, S. Metal-Organic Frameworks for $CO_2$ Chemical Transformations. *Small* **2016**, *12*, 6309−6324.

(7) Maina, J. W.; Pozo-Gonzalo, C.; Kong, L.; Schütz, J.; Hill, M.; Dumée, L. F. Metal Organic Framework Based Catalysts for $CO_2$ Conversion. *Mater. Horiz.* **2017**, *4*, 345−361.

(8) Liang, L.; Liu, C.; Jiang, F.; Chen, Q.; Zhang, L.; Xue, H.; Jiang, H.-L.; Qian, J.; Yuan, D.; Hong, M. Carbon Dioxide Capture and Conversion by an Acid-Base Resistant Metal-Organic Framework. *Nat. Commun.* **2017**, *8*, 1233.



DOI: 10.1021/acs.chemmater.8b04792
*Chem. Mater.* 2019, 31, 1084−1091

(9) Guillerm, V.; Weseliński, Ł. J.; Belmabkhout, Y.; Cairns, A. J.; D'Elia, V.; Wojtas, Ł.; Adil, K.; Eddaoudi, M. Discovery and Introduction of a (3,18)-Connected Net as an Ideal Blueprint for the Design of Metal-Organic Frameworks. *Nat. Chem.* **2014**, *6*, 673−680.
(10) Li, P.-Z.; Wang, X.-J.; Liu, J.; Lim, J. S.; Zou, R.; Zhao, Y. A Triazole-Containing Metal-Organic Framework as a Highly Effective and Substrate Size-Dependent Catalyst for $CO_2$ Conversion. *J. Am. Chem. Soc.* **2016**, *138*, 2142−2145.
(11) Dong, J.; Cui, P.; Shi, P.-F.; Cheng, P.; Zhao, B. Ultrastrong Alkali-Resisting Lanthanide-Zeolites Assembled by $[Ln_{60}]$ Nanocages. *J. Am. Chem. Soc.* **2015**, *137*, 15988−15991.
(12) Beyzavi, M. H.; Klet, R. C.; Tussupbayev, S.; Borycz, J.; Vermeulen, N. A.; Cramer, C. J.; Stoddart, J. F.; Hupp, J. T.; Farha, O. K. A Hafnium-Based Metal-Organic Framework as an Efficient and Multifunctional Catalyst for Facile $CO_2$ Fixation and Regioselective and Enantioretentive Epoxide Activation. *J. Am. Chem. Soc.* **2014**, *136*, 15861−15864.
(13) Zhu, J.; Usov, P. M.; Xu, W.; Celis-Salazar, P. J.; Lin, S.; Kessinger, M. C.; Landaverde-Alvarado, C.; Cai, M.; May, A. M.; Slebodnick, C.; Zhu, D.; Senanayake, S. D.; Morris, A. J. A New Class of Metal-Cyclam-Based Zirconium Metal-Organic Frameworks for $CO_2$ Adsorption and Chemical Fixation. *J. Am. Chem. Soc.* **2018**, *140*, 993−1003.
(14) Yuan, S.; Zou, L.; Li, H.; Chen, Y.-P.; Qin, J.; Zhang, Q.; Lu, W.; Hall, M. B.; Zhou, H.-C. Flexible Zirconium Metal-Organic Frameworks as Bioinspired Switchable Catalysts. *Angew. Chem., Int. Ed.* **2016**, *55*, 10776−10780.
(15) Gao, W.-Y.; Chen, Y.; Niu, Y.; Williams, K.; Cash, L.; Perez, P. J.; Wojtas, L.; Cai, J.; Chen, Y.-S.; Ma, S. Crystal Engineering of an nbo Topology Metal-Organic Framework for Chemical Fixation of $CO_2$ under Ambient Conditions. *Angew. Chem., Int. Ed.* **2014**, *53*, 2615−2619.
(16) He, H.; Sun, Q.; Gao, W.; Perman, J. A.; Sun, F.; Zhu, G.; Aguila, B.; Forrest, K.; Space, B.; Ma, S. A Stable Metal−Organic Framework Featuring a Local Buffer Environment for Carbon Dioxide Fixation. *Angew. Chem., Int. Ed.* **2018**, *57*, 4657−4662.
(17) Li, P.-Z.; Wang, X.-J.; Liu, J.; Phang, H. S.; Li, Y.; Zhao, Y. Highly Effective Carbon Fixation via Catalytic Conversion of $CO_2$ by an Acylamide-Containing Metal−Organic Framework. *Chem. Mater.* **2017**, *29*, 9256−9261.
(18) Liang, J.; Chen, R.-P.; Wang, X.-Y.; Liu, T.-T.; Wang, X.-S.; Huang, Y.-B.; Cao, R. Postsynthetic Ionization of an Imidazole-Containing Metal-Organic Framework for the Cycloaddition of Carbon Dioxide and Epoxides. *Chem. Sci.* **2017**, *8*, 1570−1575.
(19) Ding, M.; Jiang, H.-L. Incorporation of Imidazolium-Based Poly(ionic liquid)s into a Metal−Organic Framework for $CO_2$ Capture and Conversion. *ACS Catal.* **2018**, *8*, 3194−3201.
(20) Xu, H.; Liu, X.-F.; Cao, C.-S.; Zhao, B.; Cheng, P.; He, L.-N. A Porous Metal-Organic Framework Assembled by $[Cu_{30}]$ Nanocages: Serving as Recyclable Catalysts for $CO_2$ Fixation with Aziridines. *Adv. Sci.* **2016**, *3*, 1600048.
(21) Aguila, B.; Sun, Q.; Wang, X.; O'Rourke, E.; Al-Enizi, A. M.; Nafady, A.; Ma, S. Lower Activation Energy for Catalytic Reactions through Host-Guest Cooperation within Metal-Organic Frameworks. *Angew. Chem., Int. Ed.* **2018**, *57*, 10107−10111.
(22) Liang, J.; Xie, Y.-Q.; Wang, X.-S.; Wang, Q.; Liu, T.-T.; Huang, Y.-B.; Cao, R. An Imidazolium-Functionalized Mesoporous Cationic Metal-Organic Framework for Cooperative $CO_2$ Fixation into Cyclic Carbonate. *Chem. Commun.* **2018**, *54*, 342−345.
(23) Sun, Y.; Huang, H.; Vardhan, H.; Aguila, B.; Zhong, C.; Perman, J. A.; Al-Enizi, A. M.; Nafady, A.; Ma, S. Facile Approach to Graft Ionic Liquid into MOF for Improving the Efficiency of $CO_2$ Chemical Fixation. *ACS Appl. Mater. Interfaces* **2018**, *10*, 27124−27130.
(24) Wang, X.; Gao, W.-Y.; Niu, Z.; Wojtas, L.; Perman, J. A.; Chen, Y.-S.; Li, Z.; Aguila, B.; Ma, S. A Metal-Metalloporphyrin Framework based on an Octatopic Porphyrin Ligand for Chemical Fixation of CO2 with Aziridines. *Chem. Commun.* **2018**, *54*, 1170−1173.
(25) Li, M.; Li, D.; O'Keeffe, M.; Yaghi, O. M. Topological Analysis of Metal−Organic Frameworks with Polytopic Linkers and/or Multiple Building Units and the Minimal Transitivity Principle. *Chem. Rev.* **2014**, *114*, 1343−1370.
(26) Stock, N.; Biswas, S. Synthesis of Metal-Organic Frameworks (MOFs): Routes to Various MOF Topologies, Morphologies, and Composites. *Chem. Rev.* **2012**, *112*, 933−969.
(27) Guillerm, V.; Kim, D.; Eubank, J. F.; Luebke, R.; Liu, X.; Adil, K.; Lah, M. S.; Eddaoudi, M. A Supermolecular Building Approach for the Design and Construction of Metal−Organic Frameworks. *Chem. Soc. Rev.* **2014**, *43*, 6141−6172.
(28) Van Vleet, M. J.; Weng, T.; Li, X.; Schmidt, J. R. In Situ, Time-Resolved, and Mechanistic Studies of Metal-Organic Framework Nucleation and Growth. *Chem. Rev.* **2018**, *118*, 3681−3721.
(29) Tranchemontagne, D. J.; Mendoza-Cortés, J. L.; O'Keeffe, M.; Yaghi, O. M. Secondary Building Units, Nets and Bonding in the Chemistry of Metal-Organic Frameworks. *Chem. Soc. Rev.* **2009**, *38*, 1257−1283.
(30) Qian, J.; Jiang, F.; Su, K.; Pan, J.; Xue, Z.; Liang, L.; Bag, P. P.; Hong, M. Heterometallic Cluster-Based Indium-Organic Frameworks. *Chem. Commun.* **2014**, *50*, 15224−15227.
(31) Zheng, S.-T.; Zuo, F.; Wu, T.; Irfanoglu, B.; Chou, C.; Nieto, R. A.; Feng, P.; Bu, X. Cooperative Assembly of Three-Ring-Based Zeolite-Type Metal-Organic Frameworks and Johnson-Type Dodecahedra. *Angew. Chem., Int. Ed.* **2011**, *50*, 1849−1852.
(32) Zheng, S.-T.; Bu, J. J.; Wu, T.; Chou, C.; Feng, P.; Bu, X. Porous Indium-Organic Frameworks and Systematization of Structural Building Blocks. *Angew. Chem., Int. Ed.* **2011**, *50*, 8858−8862.
(33) Liu, Y.; Eubank, J. F.; Cairns, A. J.; Eckert, J.; Kravtsov, V. C.; Luebke, R.; Eddaoudi, M. Assembly of Metal-Organic Frameworks (MOFs) Based on Indium-Trimer Building Blocks: a Porous MOF with soc Topology and High Hydrogen Storage. *Angew. Chem., Int. Ed.* **2007**, *46*, 3278−3283.
(34) Stylianou, K. C.; Heck, R.; Chong, S. Y.; Bacsa, J.; Jones, J. T. A.; Khimyak, Y. Z.; Bradshaw, D.; Rosseinsky, M. J. A Guest-Responsive Fluorescent 3D Microporous Metal−Organic Framework Derived from a Long-Lifetime Pyrene Core. *J. Am. Chem. Soc.* **2010**, *132*, 4119−4130.
(35) Carrington, E. J.; McAnally, C. A.; Fletcher, A. J.; Thompson, S. P.; Warren, M.; Brammer, L. Solvent-Switchable Continuous-Breathing Behaviour in a Diamondoid Metal−Organic Framework and its Influence on $CO_2$ versus $CH_4$ Selectivity. *Nat. Chem.* **2017**, *9*, 882−889.
(36) Zhai, Q.-G.; Bu, X.; Mao, C.; Zhao, X.; Feng, P. Systematic and Dramatic Tuning on Gas Sorption Performance in Heterometallic Metal-Organic Frameworks. *J. Am. Chem. Soc.* **2016**, *138*, 2524−2527.
(37) Cairns, A. J.; Eckert, J.; Wojtas, L.; Thommes, M.; Wallacher, D.; Georgiev, P. A.; Forster, P. M.; Belmabkhout, Y.; Ollivier, J.; Eddaoudi, M. Gaining Insights on the $H_2$−Sorbent Interactions: Robust soc-MOF Platform as a Case Study. *Chem. Mater.* **2016**, *28*, 7353−7361.
(38) Li, Q.; Xue, D.-X.; Zhang, Y.-F.; Zhang, Z.-H.; Gao, Z.; Bai, J. A Dual-Functional Indium−Organic Framework towards Organic Pollutant Decontamination via Physically Selective Adsorption and Chemical Photodegradation. *J. Mater. Chem. A* **2017**, *5*, 14182−14189.
(39) Leng, F.; Liu, H.; Ding, M.; Lin, Q.-P.; Jiang, H.-L. Boosting Photocatalytic Hydrogen Production of Porphyrinic MOFs: The Metal Location in Metalloporphyrin Matters. *ACS Catal.* **2018**, *8*, 4583−4590.
(40) Du, X.; Fan, R.; Qiang, L.; Xing, K.; Ye, H.; Ran, X.; Song, Y.; Wang, P.; Yang, Y. Controlled $Zn^{2+}$-Triggered Drug Release by Preferred Coordination of Open Active Sites within Functionalization Indium Metal Organic Frameworks. *ACS Appl. Mater. Interfaces* **2017**, *9*, 28939−28948.
(41) Yu, P.; Li, Q.; Hu, Y.; Liu, N.; Zhang, L.; Su, K.; Qian, J.; Huang, S.; Hong, M. Cuboctahedron-Based Indium−Organic Frameworks for Gas Sorption and Selective Cation Exchange. *Chem. Commun.* **2016**, *52*, 7978−7981.


DOI: 10.1021/acs.chemmater.8b04792
*Chem. Mater.* 2019, 31, 1084−1091

(42) Hou, S.-L.; Dong, J.; Jiang, X.-L.; Jiao, Z.-H.; Wang, C.-M.; Zhao, B. Interpenetration-Dependent Luminescent Probe in Indium-Organic Frameworks for Selectively Detecting Nitrofurazone in Water. *Anal. Chem.* **2018**, *90*, 1516−1519.
(43) Joarder, B.; Lin, J.-B.; Romero, Z.; Shimizu, G. K. H. Single Crystal Proton Conduction Study of a Metal Organic Framework of Modest Water Stability. *J. Am. Chem. Soc.* **2017**, *139*, 7176−7179.
(44) Du, M.; Chen, M.; Yang, X.-G.; Wen, J.; Wang, X.; Fang, S.-M.; Liu, C.-S. A Channel-Type Mesoporous In(iii)−Carboxylate Coordination Framework with High Physicochemical Stability for Use as an Electrode Material in Supercapacitors. *J. Mater. Chem. A* **2014**, *2*, 9828−9834.
(45) Yao, S.; Wang, D.; Cao, Y.; Li, G.; Huo, Q.; Liu, Y. Two Stable 3D Porous Metal−Organic Frameworks with High Performance for Gas Adsorption and Separation. *J. Mater. Chem. A* **2015**, *3*, 16627−16632.
(46) Tan, Y.-X.; Yang, X.; Li, B.-B.; Yuan, D. Rational Design of a flu-Type Heterometallic Cluster-Based Zr-MOF. *Chem. Commun.* **2016**, *52*, 13671−13674.
(47) Deria, P.; Mondloch, J. E.; Karagiaridi, O.; Bury, W.; Hupp, J. T.; Farha, O. K. Beyond Post-Synthesis Modification: Evolution of Metal-Organic Frameworks via Building Block Replacement. *Chem. Soc. Rev.* **2014**, *43*, 5896−5912.
(48) Lu, W.; Wei, Z.; Gu, Z.-Y.; Liu, T.-F.; Park, J.; Park, J.; Tian, J.; Zhang, M.; Zhang, Q.; III Gentle, T.; Bosch, M.; Zhou, H.-C. Tuning the Structure and Function of Metal−Organic Frameworks via Linker Design. *Chem. Soc. Rev.* **2014**, *43*, 5561−5593.
(49) Zhao, X.; Bu, X.; Wu, T.; Zheng, S.-T.; Wang, L.; Feng, P. Selective Anion Exchange with Nanogated Isoreticular Positive Metal-Organic Frameworks. *Nat. Commun.* **2013**, *4*, 2344.
(50) Blatov, V. A.; Shevchenko, A. P.; Proserpio, D. M. Applied Topological Analysis of Crystal Structures with the Program Package ToposPro. *Cryst. Growth Des.* **2014**, *14*, 3576−3586.
(51) Zheng, S.-T.; Bu, J. T.; Li, Y.; Wu, T.; Zuo, F.; Feng, P.; Bu, X. Pore Space Partition and Charge Separation in Cage-within-Cage Indium−Organic Frameworks with High $CO_2$ Uptake. *J. Am. Chem. Soc.* **2010**, *132*, 17062−17064.
(52) Zheng, B.; Sun, X.; Li, G.; Cairns, A. J.; Kravtsov, V. C.; Huo, Q.; Liu, Y.; Eddaoudi, M. Solvent-Controlled Assembly of Ionic Metal−Organic Frameworks Based on Indium and Tetracarboxylate Ligand: Topology Variety and Gas Sorption Properties. *Cryst. Growth Des.* **2016**, *16*, 5554−5562.
(53) Düren, T.; Bae, Y.-S.; Snurr, R. Q. Using Molecular Simulation to Characterise Metal−Organic Frameworks for Adsorption Applications. *Chem. Soc. Rev.* **2009**, *38*, 1237−1247.
(54) Kim, J.; Kim, S.-N.; Jang, H.-G.; Seo, G.; Ahn, W.-S. $CO_2$ Cycloaddition of Styrene Oxide over MOF Catalysts. *Appl. Catal., A* **2013**, *453*, 175−180.
(55) North, M.; Pasquale, R. Mechanism of Cyclic Carbonate Synthesis from Epoxides and $CO_2$. *Angew. Chem.* **2009**, *121*, 2990−2992.



DOI: 10.1021/acs.chemmater.8b04792
*Chem. Mater.* 2019, 31, 1084−1091